CHEMISTRY OF MATERIALS

Article

Cite This: Chem. Mater. 2019, 31, 6900−6907

pubs.acs.org/cm

Even−Odd Alkyl Chain-Length Alternation Regulates Oligothiophene Crystal Structure

Edmund K. Burnett,[†,⊥] Qianxiang Ai,[‡,§,⊥] Benjamin P. Cherniawski,[†] Sean R. Parkin,[‡] Chad Risko,*[‡,§] and Alejandro L. Briseno*[†,∥]

[†]Department of Polymer Science and Engineering, University of Massachusetts Amherst, Amherst, Massachusetts 01003, United States

[‡]Department of Chemistry, University of Kentucky, Lexington, Kentucky 40506, United States

[§]Center for Applied Energy Research, University of Kentucky, Lexington, Kentucky 40511, United States

[∥]Department of Chemistry, The Pennsylvania State University, University Park, Pennsylvania 16802, United States

Supporting Information

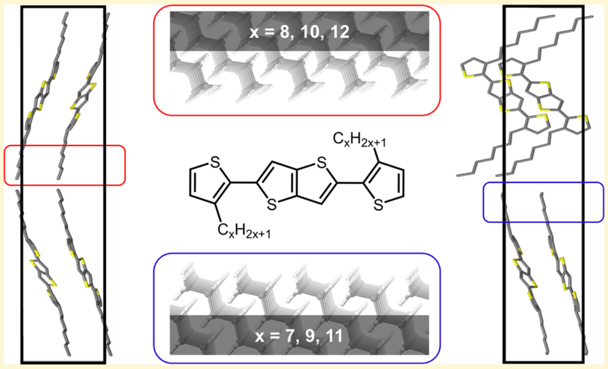

ABSTRACT: Alkyl chains of varied length and steric bulk are generally appended to π-conjugated chromophores to increase solubility. These alkyl chains also regulate many aspects of the solid-state packing and, in turn, resultant electronic and optical properties of organic semiconductors, yet there remains little understanding as to how these moieties govern such characteristics. Here, we report on a series of (2,5-bis(3-*alkyl*thiophen-2-yl)thieno[3,2-*b*]thiophenes) (BTTT) monomers where the single-crystal packing configurations and melting points alternate as a function of whether the alkyl side chains have an even or odd number of carbon atoms. When the alkyl chains contain an even number of carbon atoms, the molecules predominantly crystallize with the BTTT units of the stacked lamellae aligned in the same direction. In contrast, when the number of carbon atoms is odd, alternating lamellae are twisted with respect to their neighbors, i.e. the BTTT moieties in one layer are aligned in an orthogonal-like fashion to those in its neighboring lamellae, and the crystal melting points tend to be higher than those with the even-numbered alkyl chains. With density functional theory calculations and geometric analyses, the variations in crystal structure and thus the differences in physical properties are rationalized by an oscillating interlayer interaction that is a function of alkyl side chain atom count and length. This study characterizes an extreme case of an organic semiconductor crystal packing alternation to highlight the effect of even−odd assembly as an underutilized and under-reported handle for tuning the molecular packing of organic semiconductor materials.

INTRODUCTION

The field of organic electronics has made major breakthroughs in performance over the past decade with charge-carrier mobilities reaching 1−10 $cm^2/(V{\cdot}s)$ in organic transistors, comparable to amorphous silicon,[1,2] and single-junction organic photovoltaic devices exhibiting power conversion efficiencies >14%.[3−7] Advances in molecular and materials design, processing, and device fabrication have each contributed to this performance rise. For many years, the focus of the synthetic community was geared toward the development of novel π-conjugated backbones to control the semiconductor electronic and optical properties, as it was believed that the alkyl side chains had minimal effect on these characteristics and that they merely enabled the material solubility that is required for solution processing. Yet, due to the importance of thin film microstructure in devices, it has been shown that the alkyl side chains play a much larger role as they can serve as key contributors to govern the solid-state molecular packing, making these insulating components important chemical handles in design of functional organic semiconductors.[8−11] Many studies have methodically adjusted alkyl side chain lengths and chemistries to better understand their impact for polymer-based materials.[12−15] There is significant drawback, though, to this type of study, as polymer molecular weight variations and dispersities can lead to batch-to-batch variability, and packing frustration increases the difficulty of investigating such semiconductors with molecular resolution.

In contrast to polymers, small molecules and oligomers allow for the characterization of well-defined structures due to controlled, monodisperse synthesis and lack of chain entanglements that can frustrate packing and prevent single-

Special Issue: Jean-Luc Bredas Festschrift

Received: April 2, 2019
Revised: July 19, 2019
Published: July 22, 2019

DOI: 10.1021/acs.chemmater.9b01317
Chem. Mater. 2019, 31, 6900−6907

crystal analyses.[16−18] Such synthetic control permits the development of more detailed structure−processing−property relationships and a deeper understanding of the nuances of chemical modifications on molecular packing and microstructure that was previously inaccessible using polymer-based materials.[17,19−34] Our group has previously exploited oligomers to vary backbone lengths, namely didodecylquaterthiophene (DDQT), to understand the effects of π-conjugation length on the transition of a material from small-molecule-like to polymer.[35] In a separate study, we synthesized oligomers of poly(2,5-bis(3-*alkyl*thiophen-2-yl) thieno[3,2-*b*]thiophenes) (pBTTT) to characterize the unique interaction with fullerenes to form high-fidelity intercalated bimolecular crystals.[36,37] Here, BTTT dimers formed an intercalated system with the fullerenes, akin to that shown for the full pBTTT polymer,[38−40] with a much higher degree of crystallinity. Though use of X-ray crystal structure analysis previously inaccessible for pBTTT, the molecular arrangement and unit cell of the oligomer−fullerene cocrystal was determined with the fullerenes embedded between the side chains of the BTTT dimer. Finally, we explored the addition of side chains to BTTT oligomers, and through experimental and computational work, examined their effect on the backbone torsion angle and propensity of *anti* vs *syn* thiophene arrangements.[41]

In this study, we synthesized a series of BTTT monomers to investigate the effect of side chain length, atom count (even vs odd number of methyl groups), and terminal methyl arrangement on interlayer molecular interactions and bulk material physical properties. We found a melting point alternation that coincides with large variations in crystal packing for the even- and odd-numbered alkyl side chains: with alkyl side chains that contain an even number of carbon atoms, the molecules predominantly crystallize with the BTTT units aligned in the same direction in all lamellae. In contrast, when the number of carbon atoms in the alkyl chains are odd, each layer is twisted such that BTTT moieties in one lamellae are nearly orthogonal to those of its neighbors. Such variations are associated with distinctive interlayer interactions, as highlighted by density functional theory (DFT) investigations of the molecular packing patterns and interlayer interfaces.

Alternating solid-state packing and material behavior has been observed in *n*-alkane and end-substituted *n*-alkanes,[42−47] *n*-alkane self-assembled monolayers,[48−52] and *n*-alkane-substituted silver nanoparticles.[53] Since the 1800s, *n*-alkanes and derivatives were known to have melting points that correlate with even−odd chain alternation with a generic "packing effect" rationalization normally given as explanation.[54] This phenomenon has received more recent attention, made possible by advancements in instrumentation and characterization techniques. The melting point alternation of *n*-alkanedithiols, for instance, stems from varied packing densities that result from different interlayer interactions that arise from the terminal methyl group orientations.[47] A melting point study of layered silver alkanethiolate lamellae expanded on the importance of interlayer interactions, using precise control over layer thickness and nanocalorimetry measurements. Melting point alternation was shown for bilayer crystals, yet a stepwise increase was exhibited in single-layer studies, highlighting the influence of interlayer interactions for property alternation.[53]

Although crystal packing alternations have been shown for a wide range of materials, little attention has been paid to this effect in organic semiconductors. Few studies have synthesized odd-length side chain materials, and those that have often overlooked the possibility of a property alternation. For example, in the seminal work of Ebata et al., the synthesis and characterization of a series of C*x*-BTBT molecules with $x = 5$−14 (where x is the number of methyl units in the alkyl side chains) stated that the "d-spacing of the other (BTBT) derivatives depended on the length of the alkyl groups: with longer alkyl groups, larger d-spacings were obtained, indicating that all the derivatives take similar molecular packing structures."[55] This study grew a single crystal for the C12-BTBT and extrapolated that molecular packing to all other molecules. Yet, using their provided structural information, it can be demonstrated that the out-of-plane spacing does not increase linearly. As shown in Figure S1, a subtle yet distinct crystal-packing alternation is observed. Our BTTT monomer series, along with this previous work, presents an extreme case of this crystal packing alternation, highlighting side chain alternation as an underexplored handle to modify molecular packing.

RESULTS AND DISCUSSION

BTTT monomers were synthesized by Stille coupling of 2,5-bis(trimethylstannyl)-theino[2,3-*b*]thiophene with 2-bromo-3-*alkyl*thiophene. Alkylated thiophenes were synthesized via Kumada coupling as reported in the literature.[36,41] The chemical structures are shown in Figure 1. We note that throughout the paper, each molecule is labeled as BTTT-C*x* with *x* denoting the number of carbon atoms in the alkyl side chains.

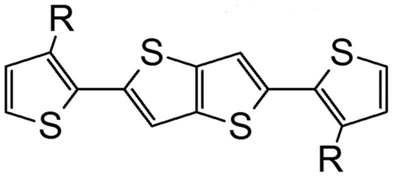

R = C_7H_{15}, C_8H_{17}, C_9H_{19}, $C_{10}H_{21}$, $C_{11}H_{23}$, $C_{12}H_{25}$

Figure 1. Structural formulas of BTTT monomers.

Optoelectronic properties as determined by UV−vis are similar across the monomer set (Figure S2). The spectra show minimal variation in absorption as a function of alkyl side chain length with a broad, featureless peak centered at 345 nm (3.59 eV). The absorption spectra of thin films spin coated from chloroform reveal a secondary peak at 425 nm (2.92 eV). An optical gap of 2.58 eV was calculated using the absorption edge with no variation seen with different side chain lengths.

Differential scanning calorimetry (DSC) was used to investigate the BTTT-C*x* thermal properties. Samples were prepared from single crystals loaded into hermetically sealed aluminum pans using heating/cooling ramps ranging from 0 to 150 °C at 10 °C/min. Melting and crystallization point alternation are present with these parameters generally increasing with increased alkyl side chain length, as shown in Figure 2. Heating and cooling curves of the BTTT-C*x* are shown in Figure S3. Such even−odd melting point alternations are well documented for *n*-alkanes[42] with even-numbered alkanes generally melting at higher temperatures than odd-numbered alkanes. However, in the case of BTTT-C*x*, this alternation is reversed with the BTTT-C*x* containing odd-numbered alkyl chains tending to have higher melting points

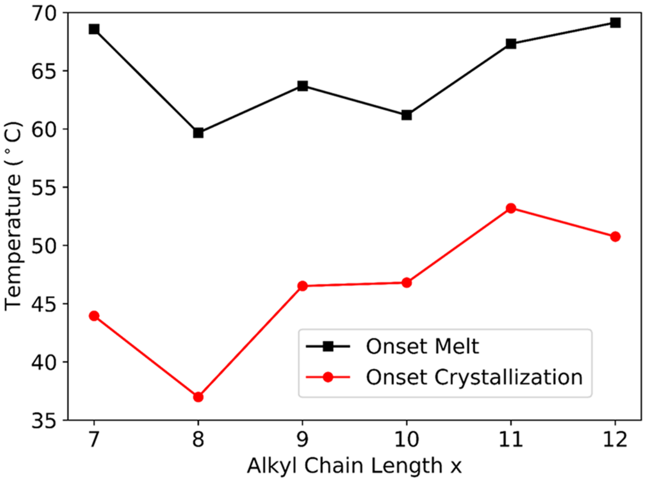

Figure 2. Onset of (squares) melting and (circles) crystallization in the BTTT monomer series; heating rate, 10 °C/min.

than those even-numbered alkyl side chains with BTTT-C12 displaying multiple melting points (though it still follows the general trend).

To investigate how chain length affects the solid-state structures of the BTTT-C*x*, single crystals were obtained from a slow evaporation of a hexane solution and analyzed by X-ray crystal structure determination. Crystals of BTTT-C*x* form as very thin, easily deformed plates/flakes. All structures consist of stacked single layers of BTTT molecules. Within each layer, the BTTT groups and the alkyl chains segregate such that BTTT groups interact solely with BTTT on quasi-parallel adjacent molecules, and the alkyl side chains interact solely with adjacent parallel alkyl chains. The refined structures of all monomer crystals exhibit two distinct conformations for the central fused thienothiophene relative to the distal alkylated thiophenes. The diffraction patterns of all crystals contain discrete diffraction spots as well as extended diffuse streaks. Depending on individual crystal quality, some streaks were smooth and featureless, whereas others were less uniform. By ignoring the diffuse streaks, all films could be indexed as primitive monoclinic with two short (∼5 Å) axes and one long (∼46−59 Å) cell axis, though the convention of defining the monoclinic (i.e., non 90°) angle led to two distinct packing types (*vide infra*), shown in Figure 3. Depending on crystal quality, however, the occasional crystal (e.g., BTTT-C9 or BTTT-C12) could be transformed to a larger C-centered monoclinic unit cell that also accounted for nonuniformity within the streaks, i.e., the additional reciprocal lattice points coincided with maxima within the streaks. For the simpler primitive setting, the refined crystal structure models each have the two BTTT conformers superimposed (i.e., disordered), whereas the centered model has the two BTTT orientations alternating within each layer. It seems likely that on a submicroscopic scale there exist domains in which the two conformers alternate, but that for diffraction from macroscopic crystals, this alternation is scrambled, leading to disorder.

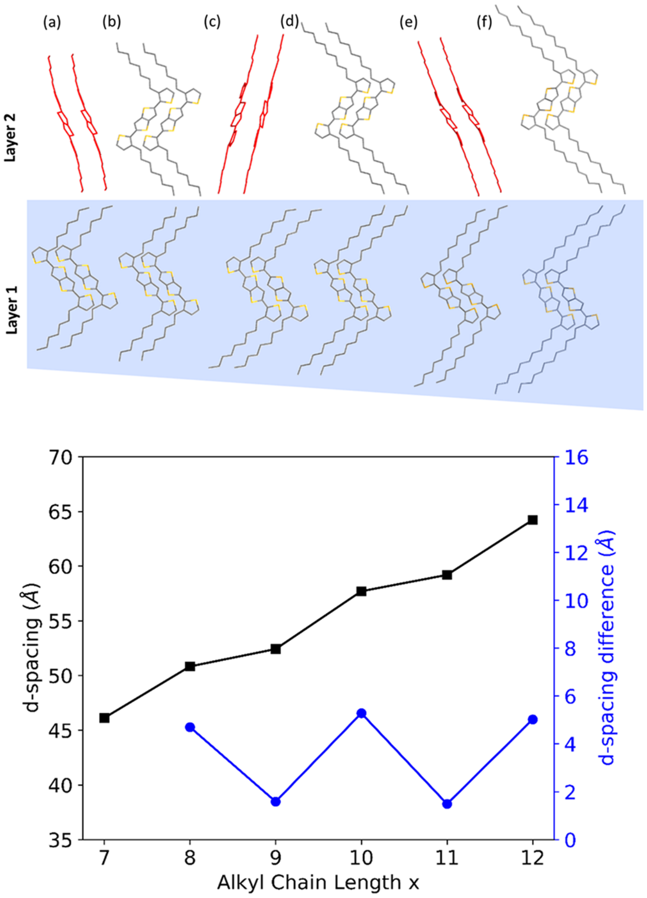

Figure 3. Top: Crystal packing motifs of, from left to right, BTTT-C7, BTTT-C8 (major), BTTT-C9, BTTT-C10, BTTT-C11, and BTTT-C12. The red molecules demonstrate the type I stacking as defined in the main text. Bottom: Along the layer stacking direction, (black) the *d*-spacing of the BTTT monomer crystals as a function of chain length, and (blue) the *d*-spacing difference with the addition of one carbon.

The comparable layer structures of all BTTT-C*x* crystals notwithstanding, the underlying crystal packing falls into two distinct types that vary in the relative orientation of adjacent layers. We initially observed that the two distinct packing types were characteristic of even−odd alkyl chain length. Crystals of the BTTT-C7, BTTT-C9, and BTTT-C11 monomers crystallize with the normal directions of the thienothiophenes in alternate BTTT layers having different orientations, a packing configuration that we refer to as type I packing. In contrast, in BTTT-C8, BTTT-C10, and BTTT-C12 crystals, the BTTT in all layers share the same orientation, a situation referred to as type II packing. One should note that such classification is not based entirely on the symmetry operations connecting the adjacent layers, as among crystals with type I packing, two different interlayer arrangements (Ia and Ib) were observed. In BTTT-C7 and BTTT-C11, the monoclinic crystals have adjacent layers related by a 2_1 screw axis along the stacking direction (Ia, space group $P2_1/c$), while for BTTT-C9, the operation is a c-glide (Ib, space group $C2/c$). Regardless of this differentiation, the interlayer interfaces of type I crystals are almost identical to each other.

We also note that we later found a few exceptions for crystals of BTTT-C8 which showed a similar c-glide operation as in type I packing; this observation was not found for any other even chain length BTTT variant. Nevertheless, the even alkyl side chain BTTT-C*x* tend to show a *preference* for type II packing over type I. In both layer stacking types, the interlayer interactions consist solely of contacts between the end methyl (even) or ethyl groups (odd) of the alkyl chains. It should be noted that these crystals/diffraction patterns were all exceedingly difficult to handle/measure, so the possibility exists that both polymorph types exist for all BTTT-Cx studied here. It is also possible that some crystals are composites that include domains with both types of layer stacking. Such a partial lack of long-range order is consistent with the presence of diffraction streaks observed in all crystals studied. Indeed, many crystals with uninterpretable, presumably composite, diffraction patterns were encountered during the crystallographic analyses.

Differences in the terminal ethyl group orientations of the alkyl chains correlate with the crystal packing and material property alternations. Here, we define $\mathbf{V}_{\mathbf{ethyl}}$ as the vector pointing from the penultimate carbon to the last carbon in the side chain. $\mathbf{V}_{\mathbf{ethyl}}$ of BTTT-Cx tend to be perpendicular to the stacking direction when x is odd, while the opposite is true when x is even. The crystal d-spacing of the plane defined by the layer stacking direction, derived as a function of increasing side chain length (Figure 3), shows an alternation pattern similar to the Cx-BTBT case.[55] The relatively tighter interlayer packings for the type I configurations, in turn, are reflected with higher melting temperatures when compared to their type II (even) counterparts.

To dig deeper into the underlying interlayer interactions of the effects due to the even or odd alkyl side chains, cohesive energies were calculated for both the 3D crystals and 2D periodic monolayers (extracted from the crystals) via periodic DFT. Here, we use the cohesive energy differences between respective 3D and 2D structures as a descriptor to estimate the strengths of interlayer interactions. The intralayer interactions are much stronger than the interlayer interactions (Figure 4), a result expected due to the considerable intralayer overlap of the π-conjugated backbones and alkyl chains. Interestingly, while the 3D and 2D intralayer interactions increase almost linearly with respect to the side chain lengths, there is a definite even−odd oscillation in the interlayer interaction.

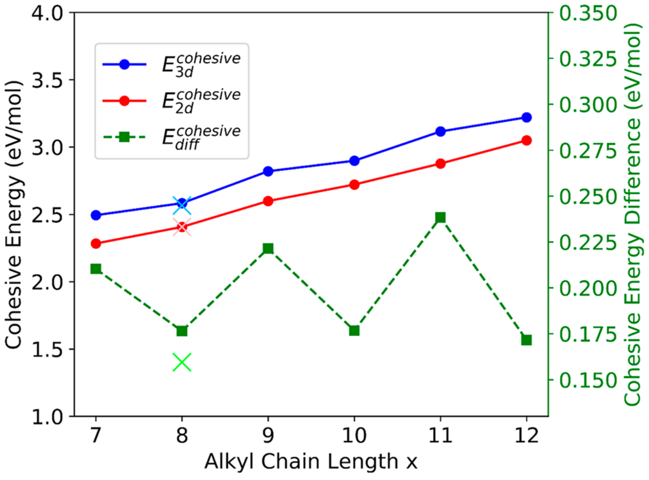

Figure 4. Cohesive energies in BTTT monomer crystals. Blue circles denote the cohesive energies of BTTT-Cx crystals; red circles denote that of monolayer BTTT-Cx, and green squares denote the difference between them. For BTTT-C8 with the type I packing, such quantities are represented by light blue, pink, and light green crosses, respectively.

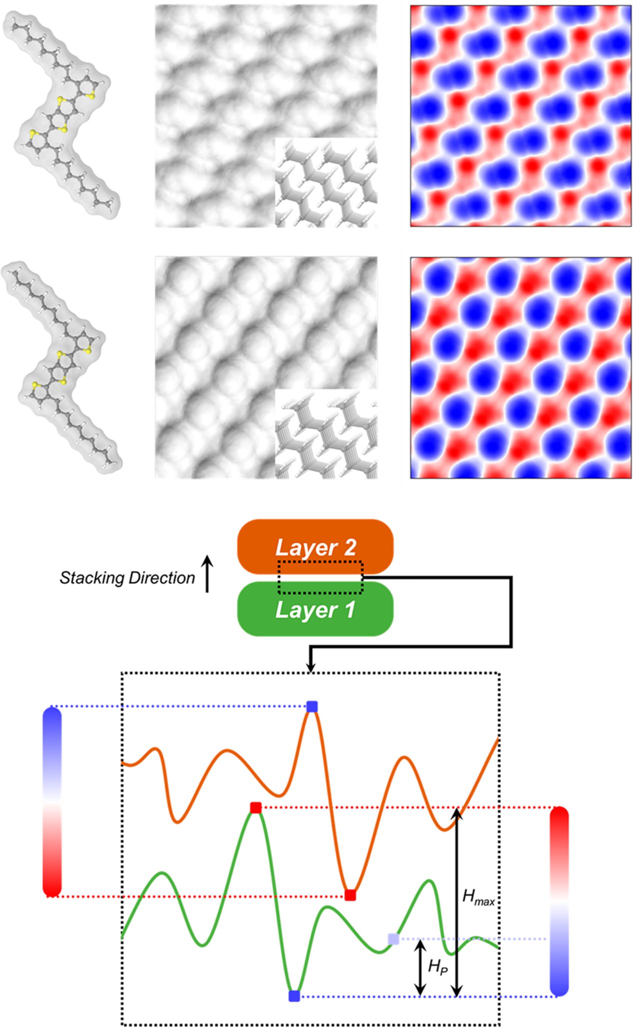

Figure 5. Representative pictorial demonstrations and color maps of the distinct, undulating alkyl-chain surface morphologies for odd (top) and even (middle) BTTT-Cx alkyl side chains. (Bottom) Color scheme for the color map of $Z(P)$: the point with $Z(P)$ = 1 is colored red, while that with $Z(P)$ = 0 is colored blue.

The difference in interlayer interactions can be, to some extent, explained by a purely geometric analysis of the alkyl chain topography at the interface. Here, we implement the concept of the solvent excluded surface, which has been used to describe the structures of macromolecules.[56,57] Through construction of the solvent excluded surface for each monolayer of BTTT-Cx, distinct undulating patterns determined by the orientation of terminal ethyl groups, thus by the parity of x, are revealed (Figure 5). To quantitatively describe the surface undulation pertaining to the interlayer interactions, the notion of normalized undulation magnitude is introduced as

$$Z_P \overset{\text{def}}{=} \frac{H_P}{H_{\max}}$$

where Z_P is the normalized undulation magnitude of point P on the surface, H_P is the undulation magnitude at point P, and $H_{\max}$ is the maximum value of H_P along a certain surface. Following the scheme in Figure 5, the surface topography can be visualized as a color map of Z_P (see the Supporting Information for further details).[58] Using the Z_P color maps of both packing types, we can illustrate the interface interactions by the value of $(Z_P^1 + Z_P^2)$ within a unit cell, where the superscripts denote individual surfaces. Such quantities describe the overlap or contact of two monolayer surfaces. If

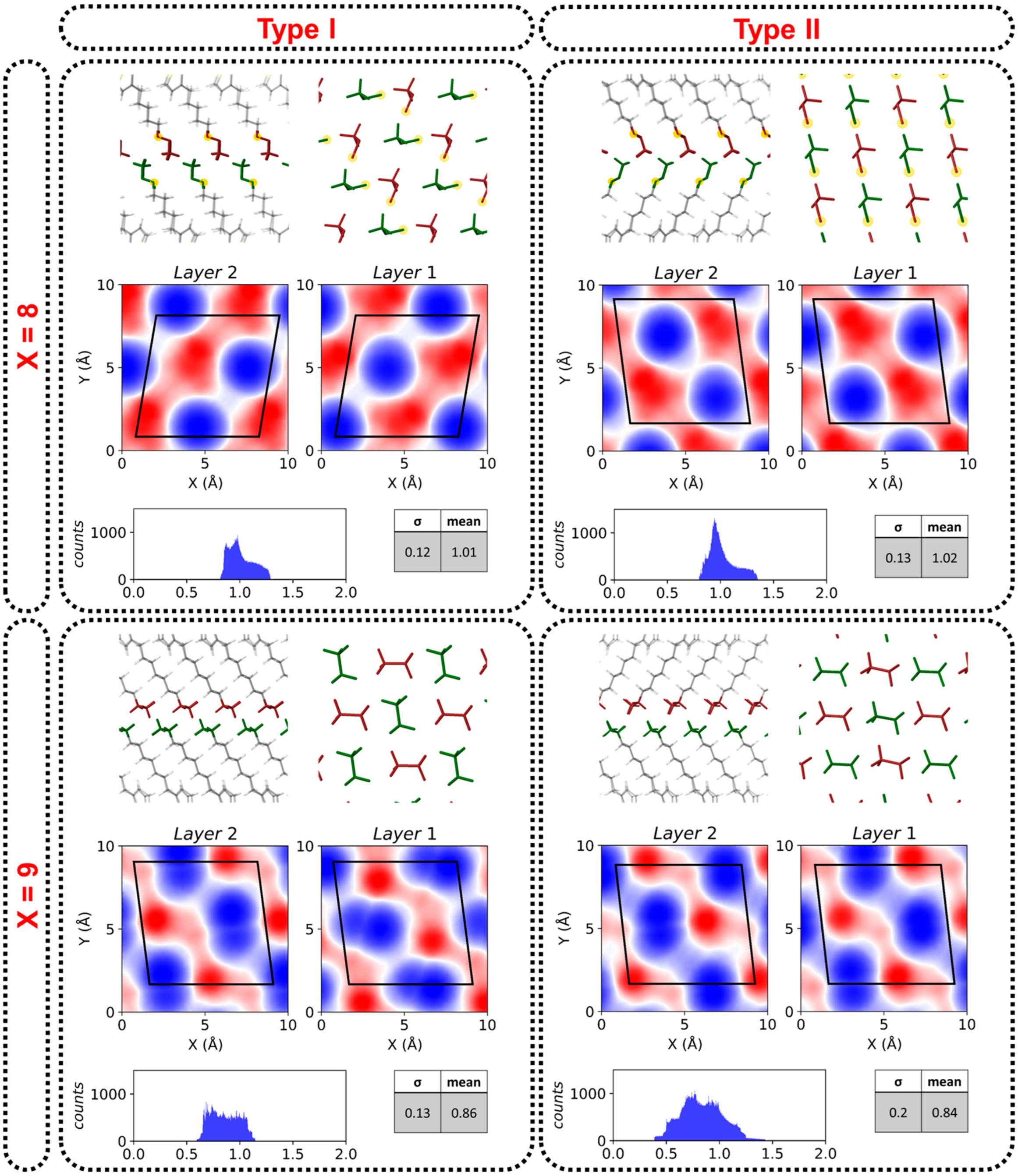

Figure 6. Comparison between BTTT-Cx type I and type II packing for x = 8 and x = 9. For each subplot, the top panel shows the side-view and the top-view for interlayer interface, where groups near the interface are colored brown or green, as shown in Figure 5. Especially for x = 8, hydrogen atoms far from the interface are removed and the third carbon (count from the end) is haloed to illustrate the orientation of alkyl chain. The middle panel shows the color map of Z_P^1 and Z_P^2, and the black parallelogram represents the corresponding unit cell. The bottom panel shows the distribution of $(Z_P^1 + Z_P^2)$ within one unit cell.

the sum of Z_P^1 and Z_P^2 is 0 (2), the spatial gap (overlap) between two molecular surfaces at point P is maximized. If the sum is 1, two surfaces merely touch at P: in this case, such a description is valid due to the existence of an inversion center in the molecule, and the absolute value of $(Z_P^1 + Z_P^2)$ is not related to any physical quantity.

Figure 6 shows the interfaces for four different crystals after periodic DFT relaxations, BTTT-C8-I, BTTT-C8-II, BTTT-C9-I, and BTTT-C9-II, where I and II denote the packing type. The experimentally determined crystal structures of BTTT-C8-I, BTTT-C8-II, and BTTT-C9-I are used as the starting point for the relaxations. For BTTT-C9-II, an *in silico* polymorph is derived by first trimming the side chains in BTTT-C10-II to C9 and then relaxing the unit-cell structure. The results of the periodic DFT relaxations are used here, in part, as it is well-known that hydrogen positions are not accurately determined by ordinary X-ray diffraction. Examination of the interlayer topographies when x = 8 shows that while the distributions of $(Z_P^1 + Z_P^2)$ within a unit cell do differ for the two packing types, the differences in the standard deviations and mean values are not significant, a result consistent with the small difference in interlayer interaction (~17 meV). When x =

9, however, the opposite situation is present: a wide distribution of $(Z_P^1 + Z_P^2)$ is found for the type II structure, and the interlayer interactions are much weaker, by ∼149 meV per molecule when compared to type I. This is consistent with the results from BTTT-C7 (Figure S4), which shares the same interlayer interface but, as mentioned, a different interlayer arrangement with respect to BTTT-C9. For $x = 7$, the type II packing configuration is determined to be ∼127 meV per molecule less stable than that for type I packing.

One plausible argument as to the variation in the surface topologies as a function of the alkyl side chain length is that the differences are strongly affected by the tilt angle of the side chains, θ, defined as the angle between the (linear) direction of alkyl chain and the layer stacking direction (usually c axis), as shown in Figure 7. It is interesting that while the even−odd effect is still present in crystals where θ is small, such as n-alkanes (θ = 15−18°),[42] no oscillation in layer stacking is observed. For BTTT-Cx, θ ranges from 42° to 45°. Hence, it seems plausible that there exists a critical value θ_c beyond which the even−odd effect is strong enough to guide layer stacking during crystallization. Notably, in C12-BTBT, θ = 30°; it would therefore be interesting to revisit the structures of Cx-BTBT to determine if similar alternating orientations are observed.[55]

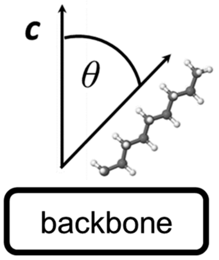

Figure 7. Definition of the alkyl side chain tilt angle, θ, where **c** is the stacking direction of molecular layers.

We return to the absence of disorder in the crystal structures of BTTT-Cx when x = 9 and 12, which is likely due to individual crystal quality. For these compounds, the diffuse diffraction streaks were not completely smooth and featureless: the streaks could be indexed and at least partially deconvoluted to yield usable (albeit noisy) diffraction data. This resulted in unit cells that were large enough to incorporate four molecules (two per asymmetric unit) without the need to model overlapped BTTT disorder. In all other cases, the unit cells (ignoring streaks) are smaller and only able to accommodate two molecules, for which it was necessary to model disorder of the BTTT cores (Figure 8). The two types of primitive cells are related by a transformation matrix. These results led us to verify the crystallographic data by computationally evaluating the relative stabilities of two well-defined structures in 2D: the "primitive" structure built from the larger unit cell, and the "supercell" structure generated by applying the aforementioned transformation to the smaller unit cell with only one disorder group. As shown in Figure 8, the primitive structure is 28−43 meV more stable than the supercell structure, which suggests that the disorder is likely a result of interlayer stacking.

■ CONCLUSION

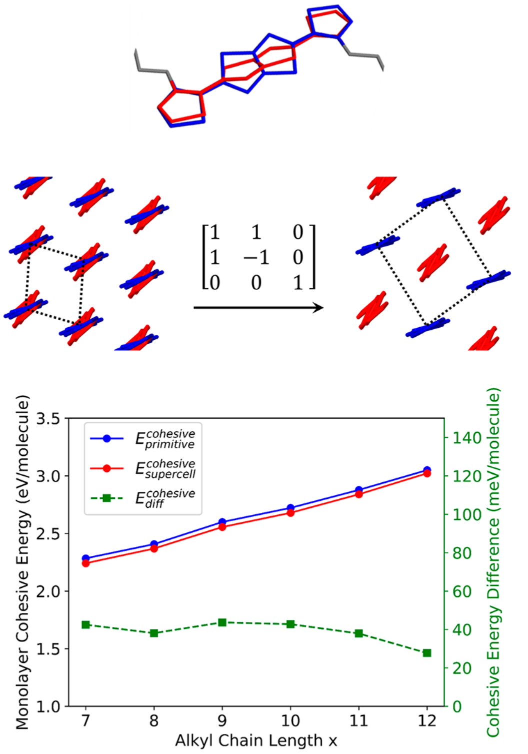

Figure 8. (Top) Pictorial representations of the disordered groups present in BTTT-C7, BTTT-C8, BTTT-C10, and BTTT-C11. (Middle) The transformation, when viewed along the long axis of BTTT, relating the "primitive" two-molecule unit cell on the left and four-molecule "supercell" on the right. Note that only one layer is shown here, while there are two layers per unit cell. (Bottom) Cohesive energies and cohesive energy differences for the two unit cells.

We synthesized and characterized a series of BTTT-Cx materials and discovered a melting point alternation brought on by crystal packing differences in which the type I packing, predominately adopted by BTTT-Cx with x being odd, exhibits an interlayer twist that enables a smaller interlayer spacing, and in turn a higher melting point. This phenomenon was further characterized with DFT and geometric investigations that demonstrated that this interlayer interaction is favorable for increasing the cohesive energy of the system and is due to the x-dependent interactions between termini of the alkyl chains. The pronounced twist, which has not been demonstrated before in systems that exhibit alternation effects, could be due to the different orientations of terminal ethyl groups ($\mathbf{V}_{\mathrm{ethyl}}$) caused by the side chain tilting angle (θ). This study characterizes an extreme case of crystal packing alternation in an organic semiconductor material to highlight the effect of even−odd assembly as an underutilized and under-reported handle for tuning the molecular packing of organic semiconducting materials.

■ ASSOCIATED CONTENT

Ⓢ Supporting Information

The Supporting Information is available free of charge on the ACS Publications website at DOI: 10.1021/acs.chemmater.9b01317.

> Detailed synthesis of BTTT-Cx monomers and ^{1}H NMR, UV−vis spectra of BTTT-Cx monomers, crystal packing alternation of the BTBT crystal, DSC thermograms of neat BTTT-Cx powders, and details of the DFT calculations (PDF)

Accession Codes

Cambridge Crystallographic Data Centre identifiers: BTTT-C7, 1860113; BTTT-C8, 1860116, 1860118; BTTT-C9, 1860117; BTTT-C10, 1860114; BTTT-C11, 1860115; BTTT-C12, ref 36.

AUTHOR INFORMATION

Corresponding Authors

*E-mail: alb818@psu.edu (A.L.B.).
*E-mail: chad.risko@uky.edu (C.R.).

ORCID

Chad Risko: 0000-0001-9838-5233
Alejandro L. Briseno: 0000-0003-2981-9143

Author Contributions

⊥E.K.B. and Q.A. contributed equally.

Notes

The authors declare no competing financial interest.

ACKNOWLEDGMENTS

E.K.B, B.P.C, and A.L.B acknowledge the Office of Naval Research (Grants N000141110636 and N0001471410053). C.R. and Q.A. acknowledge the National Science Foundation (Award DMR-1627428) for support of this work. Supercomputing resources on the Lipscomb High Performance Computing Cluster were provided by the University of Kentucky Information Technology Department and Center for Computational Sciences (CCS). Crystallography at UK was supported by the NSF (Awards MRI CHE-0319176 and CHE-1625732). We thank Dr. Kevin Gagnon at the ALS, and access to the Advanced Light Source is supported by the Director, Office of Science, Office of Basic Energy Sciences of the U.S. Department of Energy under Contract DE-AC02-05CH11231.

REFERENCES

(1) Yamashita, Y.; Hinkel, F.; Marszalek, T.; Zajaczkowski, W.; Pisula, W.; Baumgarten, M.; Matsui, H.; Müllen, K.; Takeya, J. Mobility Exceeding 10 cm2/(V·s) in Donor–Acceptor Polymer Transistors with Band-like Charge Transport. *Chem. Mater.* **2016**, *28* (2), 420–424.

(2) Paterson, A. F.; Treat, N. D.; Zhang, W.; Fei, Z.; Wyatt-Moon, G.; Faber, H.; Vourlias, G.; Patsalas, P. A.; Solomeshch, O.; Tessler, N. Small molecule/polymer blend organic transistors with hole mobility exceeding 13 cm2 V− 1 s− 1. *Adv. Mater.* **2016**, *28* (35), 7791–7798.

(3) Fei, Z.; Eisner, F. D.; Jiao, X.; Azzouzi, M.; Röhr, J. A.; Han, Y.; Shahid, M.; Chesman, A. S.; Easton, C. D.; McNeill, C. R. An Alkylated Indacenodithieno [3, 2-b] thiophene-Based Nonfullerene Acceptor with High Crystallinity Exhibiting Single Junction Solar Cell Efficiencies Greater than 13% with Low Voltage Losses. *Adv. Mater.* **2018**, *30* (8), 1705209.

(4) Li, S.; Ye, L.; Zhao, W.; Yan, H.; Yang, B.; Liu, D.; Li, W.; Ade, H.; Hou, J. A Wide Band Gap Polymer with a Deep Highest Occupied Molecular Orbital Level Enables 14.2% Efficiency in Polymer Solar Cells. *J. Am. Chem. Soc.* **2018**, *140* (23), 7159–7167.

(5) Xu, X.; Yu, T.; Bi, Z.; Ma, W.; Li, Y.; Peng, Q. Realizing Over 13% Efficiency in Green-Solvent-Processed Nonfullerene Organic Solar Cells Enabled by 1, 3, 4-Thiadiazole-Based Wide-Bandgap Copolymers. *Adv. Mater.* **2018**, *30* (3), 1703973.

(6) Zhao, W.; Li, S.; Yao, H.; Zhang, S.; Zhang, Y.; Yang, B.; Hou, J. Molecular optimization enables over 13% efficiency in organic solar cells. *J. Am. Chem. Soc.* **2017**, *139* (21), 7148–7151.

(7) Che, X.; Li, Y.; Qu, Y.; Forrest, S. R. High fabrication yield organic tandem photovoltaics combining vacuum-and solution-processed subcells with 15% efficiency. *Nature Energy* **2018**, *3* (5), 422.

(8) Mei, J.; Bao, Z. Side chain engineering in solution-processable conjugated polymers. *Chem. Mater.* **2014**, *26* (1), 604–615.

(9) Zhou, Y.; Kurosawa, T.; Ma, W.; Guo, Y.; Fang, L.; Vandewal, K.; Diao, Y.; Wang, C.; Yan, Q.; Reinspach, J. High performance all-polymer solar cell via polymer side chain engineering. *Adv. Mater.* **2014**, *26* (22), 3767–3772.

(10) Fang, L.; Zhou, Y.; Yao, Y.-X.; Diao, Y.; Lee, W.-Y.; Appleton, A. L.; Allen, R.; Reinspach, J.; Mannsfeld, S. C.; Bao, Z. Side-chain engineering of isoindigo-containing conjugated polymers using polystyrene for high-performance bulk heterojunction solar cells. *Chem. Mater.* **2013**, *25* (24), 4874–4880.

(11) Mei, J.; Kim, D. H.; Ayzner, A. L.; Toney, M. F.; Bao, Z. Siloxane-terminated solubilizing side chains: bringing conjugated polymer backbones closer and boosting hole mobilities in thin-film transistors. *J. Am. Chem. Soc.* **2011**, *133* (50), 20130–20133.

(12) Park, Y. D.; Kim, D. H.; Jang, Y.; Cho, J. H.; Hwang, M.; Lee, H. S.; Lim, J. A.; Cho, K. Effect of side chain length on molecular ordering and field-effect mobility in poly (3-alkylthiophene) transistors. *Org. Electron.* **2006**, *7* (6), 514–520.

(13) Gadisa, A.; Oosterbaan, W. D.; Vandewal, K.; Bolsée, J. C.; Bertho, S.; D'Haen, J.; Lutsen, L.; Vanderzande, D.; Manca, J. V. Effect of Alkyl Side-Chain Length on Photovoltaic Properties of Poly (3-alkylthiophene)/PCBM Bulk Heterojunctions. *Adv. Funct. Mater.* **2009**, *19* (20), 3300–3306.

(14) Chu, T. Y.; Lu, J.; Beaupré, S.; Zhang, Y.; Pouliot, J. R.; Zhou, J.; Najari, A.; Leclerc, M.; Tao, Y. Effects of the molecular weight and the side chain length on the photovoltaic performance of dithienosilole/thienopyrrolodione copolymers. *Adv. Funct. Mater.* **2012**, *22* (11), 2345–2351.

(15) Back, J. Y.; Yu, H.; Song, I.; Kang, I.; Ahn, H.; Shin, T. J.; Kwon, S.-K.; Oh, J. H.; Kim, Y.-H. Investigation of structure–property relationships in diketopyrrolopyrrole-based polymer semiconductors via side chain engineering. *Chem. Mater.* **2015**, *27* (5), 1732–1739.

(16) Zhang, L.; Colella, N. S.; Cherniawski, B. P.; Mannsfeld, S. C.; Briseno, A. L. Oligothiophene semiconductors: synthesis, characterization, and applications for organic devices. *ACS Appl. Mater. Interfaces* **2014**, *6* (8), 5327–5343.

(17) Murphy, A. R.; Frechet, J. M. Organic semiconducting oligomers for use in thin film transistors. *Chem. Rev.* **2007**, *107* (4), 1066–1096.

(18) Mishra, A.; Ma, C.-Q.; Bauerle, P. Functional oligothiophenes: molecular design for multidimensional nanoarchitectures and their applications. *Chem. Rev.* **2009**, *109* (3), 1141–1276.

(19) Mena-Osteritz, E.; Meyer, A.; Langeveld-Voss, B. M.; Janssen, R. A.; Meijer, E.; Bäuerle, P. Two-Dimensional Crystals of Poly (3-Alkyl-thiophene) s: Direct Visualization of Polymer Folds in Submolecular Resolution. *Angew. Chem.* **2000**, *112* (15), 2791–2796.

(20) Izumi, T.; Kobashi, S.; Takimiya, K.; Aso, Y.; Otsubo, T. Synthesis and spectroscopic properties of a series of β-blocked long oligothiophenes up to the 96-mer: Revaluation of effective conjugation length. *J. Am. Chem. Soc.* **2003**, *125* (18), 5286–5287.

(21) Khlaifia, D.; Ewels, C. P.; Massuyeau, F.; Chemek, M.; Faulques, E.; Duvail, J.-L.; Alimi, K. Unraveling the real structures of solution-based and surface-bound poly (3-hexylthiophene)(P3HT) oligomers: a combined theoretical and experimental study. *RSC Adv.* **2016**, *6* (61), 56174–56182.

(22) Mukhopadhyay, T.; Puttaraju, B.; Roy, P.; Dasgupta, J.; Meyer, A.; Rudnick, A.; Tscheuschner, S.; Kahle, F. J.; Köhler, A.; Patil, S. Facile Synthesis and Chain-Length Dependence of the Optical and Structural Properties of Diketopyrrolopyrrole-Based Oligomers. *Chem. - Eur. J.* **2017**, *23* (55), 13718–13723.

(23) Kan, B.; Li, M.; Zhang, Q.; Liu, F.; Wan, X.; Wang, Y.; Ni, W.; Long, G.; Yang, X.; Feng, H. A series of simple oligomer-like small molecules based on oligothiophenes for solution-processed solar cells with high efficiency. *J. Am. Chem. Soc.* **2015**, *137* (11), 3886–3893.

(24) Gadakh, S.; Shimon, L. J.; Gidron, O. Regioselective Transformation of Long π-Conjugated Backbones: From Oligofurans to Oligoarenes. *Angew. Chem.* **2017**, *129* (44), 13789–13793.

(25) Lik, A.; Jenthra, S.; Fritze, L.; Müller, L.; Truong, K. N.; Helten, H. From Monodisperse Thienyl-and Furylborane Oligomers to Polymers: Modulating the Optical Properties through the Hetarene Ratio. *Chem. - Eur. J.* **2018**, *24* (46), 11961−11972.

(26) Jin, X.-H.; Sheberla, D.; Shimon, L. J.; Bendikov, M. Highly coplanar very long oligo (alkylfuran) s: a conjugated system with specific head-to-head defect. *J. Am. Chem. Soc.* **2014**, *136* (6), 2592−2601.

(27) Lee, T.; Landis, C. A.; Dhar, B. M.; Jung, B. J.; Sun, J.; Sarjeant, A.; Lee, H.-J.; Katz, H. E. Synthesis, structural characterization, and unusual field-effect behavior of organic transistor semiconductor oligomers: inferiority of oxadiazole compared with other electron-withdrawing subunits. *J. Am. Chem. Soc.* **2009**, *131* (5), 1692−1705.

(28) Hutchison, G. R.; Ratner, M. A.; Marks, T. J. Intermolecular charge transfer between heterocyclic oligomers. Effects of heteroatom and molecular packing on hopping transport in organic semiconductors. *J. Am. Chem. Soc.* **2005**, *127* (48), 16866−16881.

(29) Lawrence, J.; Goto, E.; Ren, J. M.; McDearmon, B.; Kim, D. S.; Ochiai, Y.; Clark, P. G.; Laitar, D.; Higashihara, T.; Hawker, C. J. A Versatile and Efficient Strategy to Discrete Conjugated Oligomers. *J. Am. Chem. Soc.* **2017**, *139* (39), 13735−13739.

(30) Koch, F. P.; Smith, P.; Heeney, M. Fibonacci's route" to regioregular oligo (3-hexylthiophene) s. *J. Am. Chem. Soc.* **2013**, *135* (37), 13695−13698.

(31) Wang, L.; Zhang, X.; Zhang, J.; Tian, H.; Lu, Y.; Geng, Y.; Wang, F. Synthesis and characterization of oligo (2, 5-bis (3-dodecylthiophen-2-yl) thieno [3, 2-b] thiophene) s: effect of the chain length and end-groups on their optical and charge transport properties. *J. Mater. Chem. C* **2014**, *2* (46), 9978−9986.

(32) Zhou, C.; Liang, Y.; Liu, F.; Sun, C.; Huang, X.; Xie, Z.; Huang, F.; Roncali, J.; Russell, T. P.; Cao, Y. Chain length dependence of the photovoltaic properties of monodisperse donor−acceptor oligomers as model compounds of polydisperse low band gap polymers. *Adv. Funct. Mater.* **2014**, *24* (47), 7538−7547.

(33) Capozzi, B.; Dell, E. J.; Berkelbach, T. C.; Reichman, D. R.; Venkataraman, L.; Campos, L. M. Length-dependent conductance of oligothiophenes. *J. Am. Chem. Soc.* **2014**, *136* (29), 10486−10492.

(34) Koch, F. P. V.; Heeney, M.; Smith, P. Thermal and structural characteristics of oligo (3-hexylthiophene) s (3HT) n, n= 4−36. *J. Am. Chem. Soc.* **2013**, *135* (37), 13699−13709.

(35) Zhang, L.; Colella, N. S.; Liu, F.; Trahan, S.; Baral, J. K.; Winter, H. H.; Mannsfeld, S. C.; Briseno, A. L. Synthesis, electronic structure, molecular packing/morphology evolution, and carrier mobilities of pure oligo-/poly (alkylthiophenes). *J. Am. Chem. Soc.* **2013**, *135* (2), 844−854.

(36) Zhang, L.; Liu, F.; Diao, Y.; Marsh, H. S.; Colella, N. S.; Jayaraman, A.; Russell, T. P.; Mannsfeld, S. C.; Briseno, A. L. The good host: formation of discrete one-dimensional fullerene "channels" in well-ordered Poly (2, 5-bis (3-alkylthiophen-2-yl) thieno [3, 2-b] thiophene) oligomers. *J. Am. Chem. Soc.* **2014**, *136* (52), 18120−18130.

(37) Burnett, E. K.; Cherniawski, B. P.; Rosa, S. J.; Smilgies, D.-M.; Parkin, S.; Briseno, A. L. Breaking the Bimolecular Crystal: The Effect of Side-Chain Length on Oligothiophene/Fullerene Intercalation. *Chem. Mater.* **2018**, *30* (8), 2550−2556.

(38) Mayer, A.; Toney, M. F.; Scully, S. R.; Rivnay, J.; Brabec, C. J.; Scharber, M.; Koppe, M.; Heeney, M.; McCulloch, I.; McGehee, M. D. Bimolecular crystals of fullerenes in conjugated polymers and the implications of molecular mixing for solar cells. *Adv. Funct. Mater.* **2009**, *19* (8), 1173−1179.

(39) Miller, N. C.; Cho, E.; Gysel, R.; Risko, C.; Coropceanu, V.; Miller, C. E.; Sweetnam, S.; Sellinger, A.; Heeney, M.; McCulloch, I. Factors governing intercalation of fullerenes and other small molecules between the side chains of semiconducting polymers used in solar cells. *Adv. Energy Mater.* **2012**, *2* (10), 1208−1217.

(40) Miller, N. C.; Cho, E.; Junk, M. J.; Gysel, R.; Risko, C.; Kim, D.; Sweetnam, S.; Miller, C. E.; Richter, L. J.; Kline, R. J. Use of X-Ray Diffraction, Molecular Simulations, and Spectroscopy to Determine the Molecular Packing in a Polymer-Fullerene Bimolecular Crystal. *Adv. Mater.* **2012**, *24* (45), 6071−6079.

(41) Cherniawski, B. P.; Lopez, S. A.; Burnett, E. K.; Yavuz, I.; Zhang, L.; Parkin, S. R.; Houk, K. N.; Briseno, A. L. The effect of hexyl side chains on molecular conformations, crystal packing, and charge transport of oligothiophenes. *J. Mater. Chem. C* **2017**, *5* (3), 582−588.

(42) Boese, R.; Weiss, H. C.; Bläser, D. The Melting point alternation in the short-chain n-alkanes: single-crystal x-ray analyses of propane at 30 K and of n-butane to n-nonane at 90 K. *Angew. Chem., Int. Ed.* **1999**, *38* (7), 988−992.

(43) Thalladi, V. R.; Nüsse, M.; Boese, R. The melting point alternation in α, ω-alkanedicarboxylic acids. *J. Am. Chem. Soc.* **2000**, *122* (38), 9227−9236.

(44) Thalladi, V. R.; Boese, R.; Weiss, H. C. The Melting Point Alternation in α, ω-Alkanediols and α, ω-Alkanediamines: Interplay between Hydrogen Bonding and Hydrophobic Interactions. *Angew. Chem., Int. Ed.* **2000**, *39* (5), 918−922.

(45) Vishweshwar, P.; Nangia, A.; Lynch, V. M. Molecular complexes of homologous alkanedicarboxylic acids with isonicotinamide: X-ray crystal structures, hydrogen bond synthons, and melting point alternation. *Cryst. Growth Des.* **2003**, *3* (5), 783−790.

(46) Bond, A. D. On the crystal structures and melting point alternation of the n-alkyl carboxylic acids. *New J. Chem.* **2004**, *28* (1), 104−114.

(47) Thalladi, V. R.; Boese, R.; Weiss, H.-C. The melting point alternation in α, ω-alkanedithiols. *J. Am. Chem. Soc.* **2000**, *122* (6), 1186−1190.

(48) Tao, F.; Bernasek, S. L. Understanding odd− even effects in organic self-assembled monolayers. *Chem. Rev.* **2007**, *107* (5), 1408−1453.

(49) Heister, K.; Rong, H.-T.; Buck, M.; Zharnikov, M.; Grunze, M.; Johansson, L. Odd− Even Effects at the S-Metal Interface and in the Aromatic Matrix of Biphenyl-Substituted Alkanethiol Self-Assembled Monolayers. *J. Phys. Chem. B* **2001**, *105* (29), 6888−6894.

(50) Thuo, M. M.; Reus, W. F.; Nijhuis, C. A.; Barber, J. R.; Kim, C.; Schulz, M. D.; Whitesides, G. M. Odd− even effects in charge transport across self-assembled monolayers. *J. Am. Chem. Soc.* **2011**, *133* (9), 2962−2975.

(51) Stoliar, P.; Kshirsagar, R.; Massi, M.; Annibale, P.; Albonetti, C.; de Leeuw, D. M.; Biscarini, F. Charge injection across self-assembly monolayers in organic field-effect transistors: Odd− even effects. *J. Am. Chem. Soc.* **2007**, *129* (20), 6477−6484.

(52) Akkerman, H. B.; Mannsfeld, S. C.; Kaushik, A. P.; Verploegen, E.; Burnier, L.; Zoombelt, A. P.; Saathoff, J. D.; Hong, S.; Atahan-Evrenk, S.; Liu, X. Effects of Odd−Even Side Chain Length of Alkyl-Substituted Diphenylbithiophenes on First Monolayer Thin Film Packing Structure. *J. Am. Chem. Soc.* **2013**, *135* (30), 11006−11014.

(53) de la Rama, L. P.; Hu, L.; Ye, Z.; Efremov, M. Y.; Allen, L. H. Size Effect and Odd−Even Alternation in the Melting of Single and Stacked AgSC n Layers: Synthesis and Nanocalorimetry Measurements. *J. Am. Chem. Soc.* **2013**, *135* (38), 14286−14298.

(54) Baeyer, A. Ueber regelmässigkeiten im schmelzpunkt homologer verbindungen. *Ber. Dtsch. Chem. Ges.* **1877**, *10* (2), 1286−1288.

(55) Ebata, H.; Izawa, T.; Miyazaki, E.; Takimiya, K.; Ikeda, M.; Kuwabara, H.; Yui, T. Highly soluble [1] benzothieno [3, 2-b] benzothiophene (BTBT) derivatives for high-performance, solution-processed organic field-effect transistors. *J. Am. Chem. Soc.* **2007**, *129* (51), 15732−15733.

(56) Lee, B.; Richards, F. M. The interpretation of protein structures: estimation of static accessibility. *J. Mol. Biol.* **1971**, *55* (3), 379−IN4.

(57) Hanson, R. M. Jmol−a paradigm shift in crystallographic visualization. *J. Appl. Crystallogr.* **2010**, *43* (5), 1250−1260.

(58) Ai, Q. wavemap. *Zenodo*; 2019